Next-generation embedded printed sensors for near-field monitoring of high-performance composites

Barragán, José; Kell, Arnold; Liu, Xiangyang; Shin, Seokjee; Mandache, Catalin; Djokic, Drazen; Bennett, Dayna; Houlahan, Katherine; Genest, Marc; Lessard, Benoît H.; Paquet, Chantal

Publisher's version / Version de l'éditeur:

https://doi.org/10.1002/adem.202401332

Advanced Engineering Materials, 27, 4, 2025-01-10

ADVANCED ENGINEERING MATERIALS
www.aem-journal.com

Next-Generation Embedded Printed Sensors for Near-Field Monitoring of High-Performance Composites

*José Barragán, Arnold Kell, Xiangyang Liu, Seokjee Shin, Catalin Mandache, Drazen Djokic, Dayna Bennett, Katherine Houlahan, Marc Genest, Benoît H. Lessard, and Chantal Paquet**

Monitoring the structural health of composites during manufacturing and in-service is desirable to alert against damage or deterioration of conditions beyond an acceptable level. Wireless sensors embedded into materials that can endure the forming and curing of carbon fiber-reinforced polymer laminates will open the door to automated near-field detection of key metrics such as temperature, strain, and manufacturing defects. Current sensing technologies are generally too intrusive and fragile to be reliably embedded into laminates or too expensive to be applied commercially. The development of embedded, low-weight, small-footprint sensors is reported here, and how these sensors can be used to monitor ply movement during the manufacturing process is demonstrated. These screen-printed sensors consist of closed-loop spiral coils excited externally with an AC magnetic field to generate a secondary field, which alerts on the change of relative position of each ply. This proof-of-concept work demonstrates how printed coil sensors can be fabricated to generate a high electromagnetic response, while minimizing their footprint in the laminate. It is determined that stacked silver coils, which are subsequently plated with copper to increase the conductance, are capable of producing signals that can be detected through over 3 mm of composite material.

1. Introduction

Carbon fiber-reinforced polymers (CFRP) are widely used as structural materials in aerospace, automotive, and naval sectors, to reduce vehicle weight and fuel consumption. This is mainly due to their superior specific strength and stiffness properties. Most commonly, these parts are made manually by sequentially laying up carbon fiber preimpregnated in thermosetting matrix (prepreg) plies over shaped tools and curing them in autoclaves.[1] One attractive processing improvement over this complex and error-prone process is forming, where the flat preforms are first assembled offline and then formed into complex 3D shapes, as defined by the mold geometry. Unlike metal forming processes, which involve plastic deformation of homogeneous materials, composite forming relies on inducing targeted inter- and inner-ply-slip. However, this is a sensitive process, and if not conducted properly, it can cause a range of adverse effects, such as corner thickening/thinning or ply wrinkling, which compromises the structural integrity of the part. These defects are difficult to mitigate due to challenges in detecting and predicting how these evolve during forming. Hence, sensing relative ply motion is key to understanding and avoiding the formation of defects. Postmanufacturing, the composite material will also endure thermal and mechanical stresses throughout its life cycle. To enhance the performance of the next-generation composite materials, wireless sensors that function with common nondestructive evaluation technologies could be easily embedded into laminates.[2]

Sensors, once seamlessly embedded into a CFRP part, can allow for strict control and verification of its condition or enable advancements in laminate technology. They can be used to monitor the health of the composite material and alert to the presence of matrix microcracks, delamination, and other critical

J. Barragán, B. H. Lessard
Department of Chemical and Biological Engineering
University of Ottawa
161 Louis Pasteur, Ottawa, ON K1N 6N5, Canada

The ORCID identification number(s) for the author(s) of this article can be found under https://doi.org/10.1002/adem.202401332.

DOI: 10.1002/adem.202401332

J. Barragán, A. Kell, X. Liu, S. Shin, D. Bennett, K. Houlahan, C. Paquet
Security and Disruptive Technologies Research Centre
National Research Council Canada
100 Sussex Dr, Ottawa, ON K1A 0R6, Canada
E-mail: Chantal.Paquet@nrc-cnrc.gc.ca

C. Mandache, D. Djokic, M. Genest
Aerospace Research Centre
National Research Council Canada
1200 Montreal Rd, Ottawa, ON K1A 0R6, Canada

B. H. Lessard
School of Electrical Engineering and Computer Science
University of Ottawa
800 King Edward Ave, Ottawa, ON K1N 6N5, Canada

defects.[3–12] They can also be used to monitor vibrations[13] or strains in material, statically or dynamically.[5,14–18]

Current embedded sensor technologies used to monitor the health of CFRP and similar composite materials suffer from poor durability and are vulnerable to temperature changes experienced during manufacturing and throughout their life cycle. For example, fiber Bragg grating (FBG) (fiber optic based) sensors have elevated costs and are complex to develop, and their measurements can be compromised by temperature changes and require additional hardware, while also being difficult to maintain.[14,19,20] Piezoresistive material-based sensors can be depolarized at the high temperatures used during the manufacturing process of CFRP, have poor homogeneity in manufacturing, and may fail when facing stresses and conditions that are inherent to aerospace materials.[4,9,13,21] Even more advanced systems, which combine both FBG and piezoresistive materials, can be used for damage detection. However, they still require complex electronics, expensive materials, and advanced algorithms, making them difficult to implement at larger scales. Nonetheless, they can achieve position accuracies between 5 and 25 mm for damage detection.[22]

Furthermore, once embedded they all have dimensions commensurate or larger than those within the defect inclusion threshold of 161 mm^2, which means that if used for commercial applications the composite piece would be considered defective.[9] Similarly, there are several innovations in the field of printed electronics integrated with CFRP. They vary greatly in application, from deicing on unmanned air vehicle (UAV) wings,[23] to damage detection using printed copper and silver electrodes.[24,25] However, these breakthroughs can only be applied to the surface of the CFRP, leaving it vulnerable to weather erosion, in addition to requiring the buffing of the top layer of epoxy in order to adhere correctly, thereby damaging the surface. To summarize, printed electronics usually only focus on the CFRP at a surface level, whereas embedded technologies can give better insight but tend to reduce the CFRP performance and entail additional cost or weight. Therein lies the novelty of the presented research, which combines the superior insight of fiber optic-based solutions, the simplicity of printed electronics, and importantly with minimal to no penalty to the structural integrity of the composite.

To better monitor the state of CFRP, a new system must be developed. The monitoring system requires the following: ability to accurately indicate ply position (from which ply migration can be inferred), not be invasive (i.e., not affect ply behavior, be compatible with the forming process, and be small enough to not be considered an inclusion), able to provide continuous measurements, be durable (survive forming, curing, and other post-processes), and able to provide qualitative and quantitative data. Printable sensors present an attractive solution to the sensors, as they could be wirelessly read, are inexpensive to manufacture, and fall below the threshold size of an inclusion.

Printed conductive coils that are embedded at critical locations within various layers of the composite materials have the ability to act as inexpensive and effective near-field sensors. The coils generate a magnetic field when externally stimulated, which can be remotely detected.[26] The detected field can provide information regarding the relative position of the sensor, temperature, or strain. Eddy current technologies, an industry-standard technology for nondestructive testing, could be leveraged for this purpose. The technique is based on electromagnetic induction and can detect very small defects in metals.[27–29] Therefore, this commonly used nondestructive evaluation method, if applied to the detection of embedded sensors within a composite, would result in a reduced need for new testing equipment and training requirements. Using this detection technology, the electromagnetic response of the sensor can be measured periodically throughout the life of the composite material (a much less conductive medium than the sensors) to monitor its structural health. Effective sensors should have the following features: 1) coils that are tightly wound, with minimal turns to ensure the sensors have a small footprint and minimize their invasiveness within the laminate; 2) high electrical conductance to generate a sufficiently strong signal to be detected through the composite and at a given standoff distance; and 3) sufficient durability to withstand the process of forming and curing.

In this study, we report the design and optimization of screen-printed sensors that have high signal output, survivability to the forming and curing conditions, minimal physical area, height, and weight, resulting in minimal impact on the laminate behavior and integrity. Furthermore, the usage of screen printing, an inexpensive manufacturing method, would allow for commercial production at larger scales. We also describe the material architectures of ply sensors that can generate sufficient magnetic responses for wireless monitoring using eddy current technologies. The method uses screen-printed molecular silver inks that have high printing resolution and low film thickness ensuring the sensors maintain a small footprint within the laminate.[30] The material architectures are developed to increase the electrical performance amplifying the sensor sensitivity. Using real forming and curing trials, we demonstrate the sensors maintain their properties and provide location data with an accuracy higher than 0.25 mm. The approach to sensing has been optimized and opens up the opportunity to further miniaturize the sensors and increase performance. The proposed work here is unique, as it puts forward a new approach to noncontact and in situ monitoring of CFRP manufacturing, and it paves the way for printed embedded sensors in structural health monitoring using convenient nondestructive techniques.

2. Results and Discussion

The experimental procedure uses CFRP-embedded planar spiral coils excited and sensed via electromagnetic induction with a transmit–receive eddy current probe scanning the composite part. **Figure 1**a shows the experimental setup of the EC NDT equipment, with the bottom representing the coil and the top representing the inductor. Their signal strength increases with the number of turns in a coil.[27] Therefore, to ensure the sensors maintain a small footprint and generate a signal that could be detected through the composite with at least a 3 mm standoff distance, the coils were designed to have tightly wound turns. We found coils with nominal line width of 300 μm and line spacing of 100 μm afforded sensors with a high turn density without causing adjacent lines of the coil to short as a result of ink slumping.

A set of coils were designed with varying numbers of turns, ranging from 1 turn (at 1.78 cm in linear length and 2 mm in

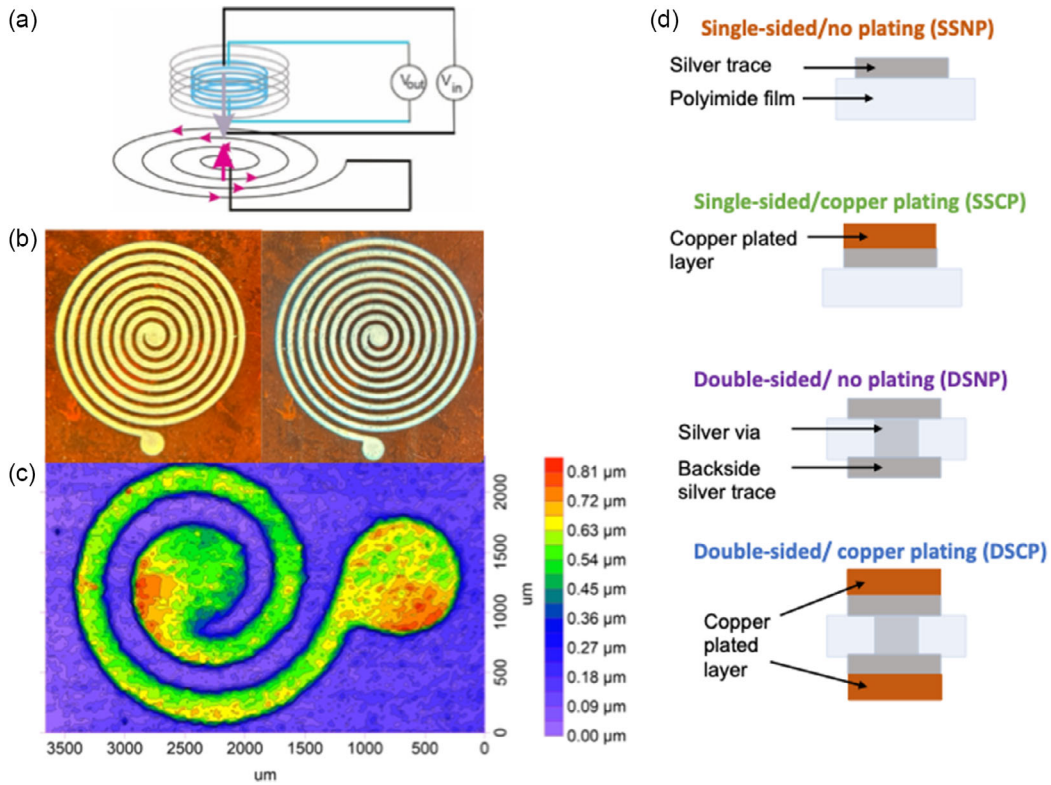

Figure 1. a) EC testing setup: Probe has signal reading (gray) and emitting (blue) components to measure the output (pink) from the spiral sensor. b) 7- and 8-turn nonplated sensor. c) Topography of a 1-turn sensor. d) Proposed architectures for spiral sensors.

diameter) to 9 turns (16.76 cm in linear length and 10 mm in diameter) with constant nominal line width and line spacing. Figure 1b shows a coil design with 7 and 8 turns, and Figure 1c shows the topography of a 1-turn sensor; in practice, it is slightly more than 1 turn, but for the purposes of this work, turns are defined as the number of lines between the base and the center. The baseline sensor architecture consisted of coils printed with silver molecular ink on polyimide film and is referred to as a single-sided nonplated sensor (SSNP). In addition to this sensor structure, three other sensor architectures were explored, as illustrated in Figure 1d. The baseline sensor, SSNP, was copper plated for 120 min yielding single-sided copper-plated (SSCP) sensors. Alternatively, coils were printed on both sides of the substrate to obtain a higher turn density for an identical size, producing double-sided nonplated (DSNP) sensors. Lastly, a combination of the former and latter approaches was used to yield double-sided copper-plated (DSCP) sensors.

The signal output from these sensors will be governed by the overall conductance and number of turns per coil. Low resistivity and low resistance (i.e., high conductance) traces are desirable because they would allow a higher induced current to flow through their turns. Despite the low volume resistivity that can be achieved with silver traces, the method of screen-printing limits how much ink can be deposited and therefore sets an upper limit on the thickness of the silver trace, capping the achievable conductance. Increases in the trace thickness would significantly improve the sensor performance with only marginally increasing the total volume of the sensor. Copper electroless plating was used as a means to increase the trace thickness and conductance to improve the sensor performance. Copper plating is particularly attractive as it deposits metal over top of the silver seed layer with limited growth laterally and therefore would not cause the lines to widen and shorten. In this work, the amount of copper deposited to the traces was tuned by controlling the plating time, offering a way to balance the quality of the sensors with conductance. The amount of copper deposited in a given time period depends on the solution and can range from $5\,\mu m\,h^{-1}$ for certain commercial products to $8\,\mu m\,h^{-1}$ for high-concentration solutions.[31] The copper plating solution used in this work had low concentrations of precursors, depositing at a low rate of $0.32\,\mu m\,h^{-1}$ and ensuring a uniform copper film formed. Coils were plated for 30, 60, and 120 min. Above 120 min of plating, the quality of plated copper degraded. **Figure 2**a shows the profile of plated and nonplated traces and confirms that the copper layer does not grow laterally, maintaining similar trace widths. The silver traces were found to have average heights of $0.58 \pm 0.06\,\mu m$. Following 20 min of copper plating, the height of the coils increases to at least 1.5 µm from the initial 0.6 µm. Prior to copper plating, the silver traces had a volume resistivity of 90 µΩ cm, a value higher than that found in literature of 15–45 µΩ cm.[32] This difference is due to the higher content of polymer binder in the ink that was added to ensure the traces survive the copper plating process. Figure 2b also shows the significant decrease in resistance and volume

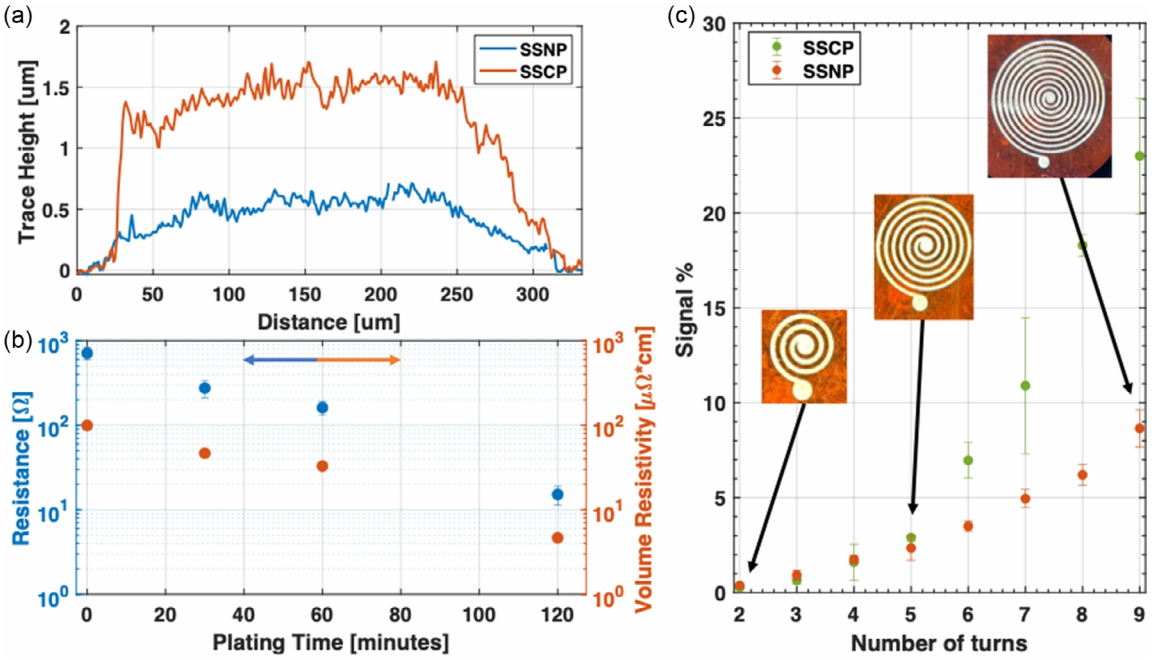

Figure 2. a) Height profile of traces from a silver- (SSNP) and copper-plated (SSCP) sensor. The copper plating increasing the thickness while keeping the width constant; b) changes in the traces resistance and volume resistivity with copper plating time; c) the signal readout of the sensors with different numbers of turns for copper-plated (SSCP) and noncopper-plated single-sided (SSNP) sensors (measurements were performed with a 1 mm stand-off between the sensors and the probe).

resistivity with increasing plating times. The resistivity decreases to a value of 4.66 μΩ cm, about 2.7 times higher than pure copper (1.72 μΩ cm ADDIN ZoTERO_TEMP).[33]

The signal strength is predicted to increase with the number of turns[27] and with decreasing resistance (increasing conductance) of the traces. The dependence of the number of turns on the signal output was evaluated at a separation of 1 mm for sensor architectures SSNP and SSCP. The results, found in Figure 2c, reveal the tradeoff between the size or footprint of sensor and its signal strength, as previously shown by Ditchurn et al.[27] The signal readout increases exponentially with the number of turns/coil for both SSNP and SSCP sensors. For instance, the 5-turn SSNP sensor has a signal of around 2% while the 9-turn sensor has a signal of 8.65%. Copper plating is shown to further improve sensor performance, as shown in the signal enhancement for the SSCP series. The relative improvement imparted by copper plating increases with the number of turns in the sensor. In this case, the 5-turn sensor has a signal of 3% (a relative 50% increase over the SSNP analog) while the 9-turn sensor has a readout of 23% (or a relative 266% increase over the SSNP analog). The significant tradeoff between sensor performance and footprint is especially important as large sensors can compromise the structural integrity of the composite.

Using sensors with 9 turns (10 mm in diameter), the different architectures (SSNP, SSCP, DSNP, and DSCP) were compared. As shown in **Figure 3**a, the sensor architecture has a strong impact on signal output. As mentioned in the experimental section, the signal output percentage consists of the ratio between energy emitted and recovered by the probe. For instance, the SSNP, SSCP, DSNP, and DSCP had signal outputs of 17.5, 30.3, 34.0, and 56.3% respectively, demonstrating that the signal for the sensors with the DSCP architecture is around 4 times higher than the SSNP. Additionally, the copper-plated (SSCP) and the double-side sensor with no copper plating (DSNP) show statistically identical increases in performance for the sensor, ≈2 times the baseline (SSNP) sensor. The DSCP sensors outperform all other sensor architectures highlighting how copper plating and stacking coils by printing on two sides of the substrates can be combined to significantly boost the signal output without significantly increasing the size of the sensors (i.e., increase in thickness of about 1 μm compared to the 50 μm thickness of the polyimide film).

The signal strength is predicted to decrease exponentially with distance,[34] underlying the need for efficient sensors to monitor through thick laminates or at large standoff distances. Therefore, these sensors were also evaluated at separation distances ranging from 1 to 4 mm from the measurement probe. This measurement is critical given that one of the objectives for this study is to obtain a readable signal from at least 3 mm separation. Results for this measurement are found in Figure 3b and confirm that the signal decreases exponentially as separation from the sensor increases as predicted by Tumanski.[34] Despite the exponential decrease in signal, all architectures remain readable at 4 mm stand-off from the coil's plane. The DSCP has the highest performance due to the implementation of both signal-enhancing techniques (more turns and lowest resistance). Three key trends of sensor behavior can be established from this data: (1) high number of turns per coil and lower resistance resulted in a higher signal output; 2) features of the sensor architectures can be combined to create a very high-performing

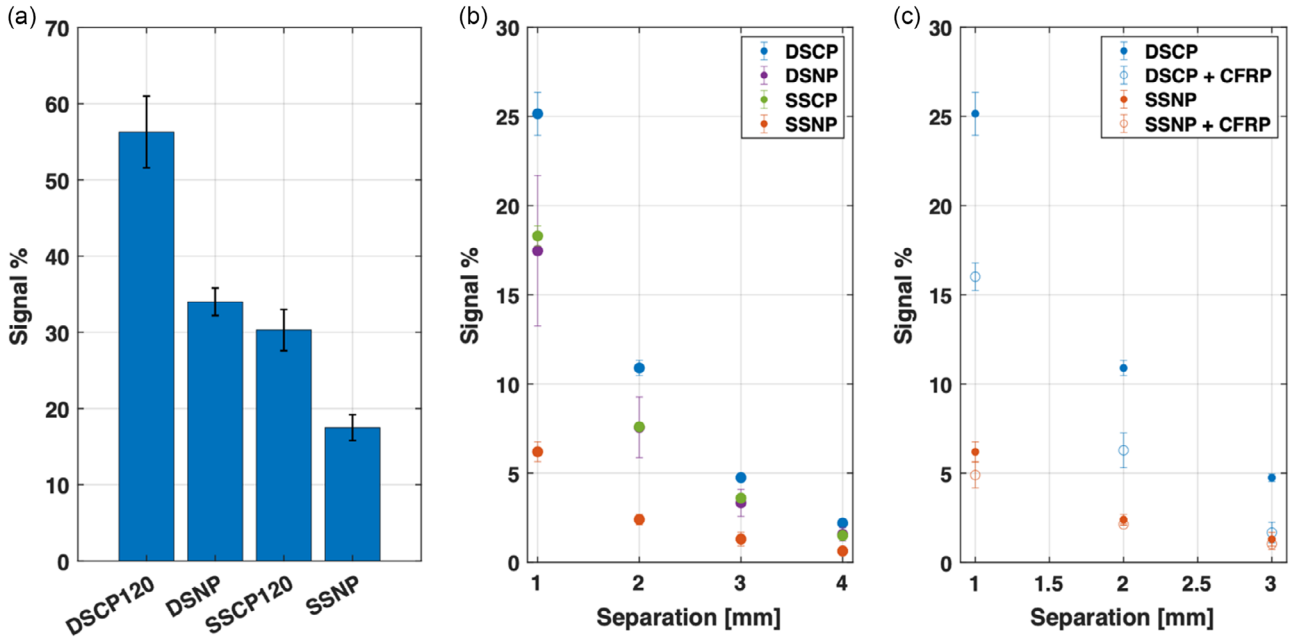

Figure 3. a) Signal readout for 9-turn sensors with different architectures measured at 0 mm between the probe and the sensor. b) Signal readout for 9-turn sensors with different architectures from 1 to 4 mm distances between the probe and the sensor. c) Signal readout for 9-turn sensors with different architectures with a piece of CFRP with thicknesses of 1–3 mm.

sensor; and 3) the signal had an exponential decrease as separation from the probe increased.

Before embedding sensors into laminates, the impact of the CFRP laminate layer on them was investigated. Because there is no precedent for the extent to which CFRP decreases the signal for passive sensors of this kind (making the obtained measurements even more critical for future near-field sensors of similar architectures), the baseline SSNP sensor and the top-performing architecture, DSCP, with 9 turns were measured at different distances, with and without a CFRP sheet of a width equal to the separation distance placed in between the probe and the sensor. Figure 3c shows the results of the measurements, which found that dampening can vary between 30 and 60% in comparison to air and was much more noticeable for the better-performing sensor. This dampening is consistent with the fact that CFRP acts as a shielding layer with resistivity of 0.022 and 310 mΩ m along and across the fibers respectively.[35] Despite the reduction in signal, the sensors still have sufficiently strong signal output to be embedded into the laminates. For instance, at 3 mm standoff distance, the DSCP sensor had its 4.75% signal strength reduced to ≈2% with the CFPR panel above it.

For the forming and curing trials, four 9-turn SSNP sensors were embedded in a CFRP test part to test the survivability and performance of the sensors. **Figure 4**a shows the three stages of the process in which the CFRP piece was scanned: 1) laminate, where the plies are assembled into a flat preform and the sensors embedded; 2) forming, where the preform is deformed to a desired shape with application of external heat and force; and 3) curing, where the piece is heated up in an autoclave and becomes rigid. An eddy current scan of the piece was taken at each step to compare the position of the embedded sensors and to verify that the sensor remains functional during harsh manufacturing conditions. The sensors were placed between plies of a preimpregnated sheet at various depths, with 3 additional sensors embedded at static positions to serve as references (R1, R2, and R3P1D). Figure S3 and S4, Supporting Information, show the structural spar that was embedded with the sensors. Figure 4b shows the superimposed scanned position of the 4 sensors at each step, with red, blue, and green representing the uncured, formed, and cured manufacturing steps, respectively. The sensors (9-turn coils, SSNP architecture) labeled A, B, C, and D were embedded at depths ranging from 0.135 up to 3.375 mm, with more displacement expected at shallower depths due to the geometry of the formed CFRP piece. The black square below the schematic represents the scanned surface and shows the displacement of the sensors at a millimeter scale. Figure S5, Supporting Information, presents a more visual representation of the ply migration during forming. Figure 4c shows the displacement of each sensor as a function of their embedding depth. The experimental results were compared with the theoretical displacement expected out of each ply and show an accuracy of ±0.6 mm (represented by the error bar), which could be further decreased to ±0.15 mm (the minimum step of the probe) with additional scans, though precision optimization was beyond the scope of this article. Whereas this technique is less accurate than X-ray equipment, which can have resolutions down to 0.015–0.2 mm,[36] it does not require embedding metal wires into the composite (which affects the structural integrity) nor specialized and expensive X-ray equipment. In contrast, EC NDT equipment is readily available and already used for other testing such as turbine blade damage[37] and would just require a change of settings in order to be able to read the sensors correctly.

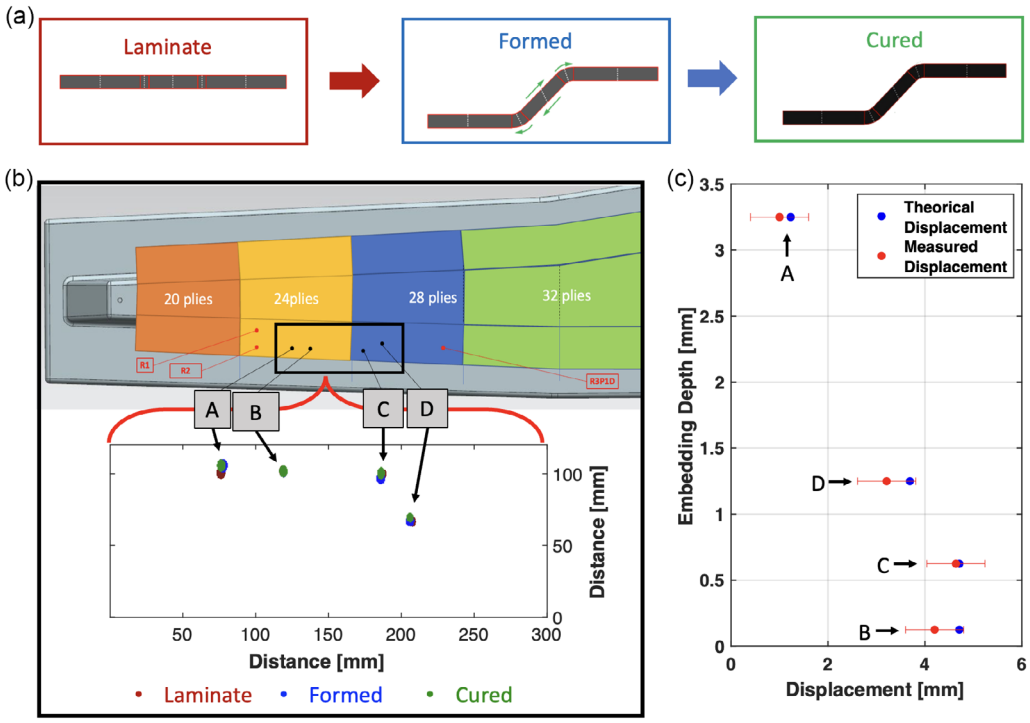

Figure 4. a) Illustration of a CFRP laminate cross section at different manufacturing stages, showing possible ply migration with green arrows. b) Schematic showing the lateral location of four 9-turn SSNP sensors, each represented by a letter (top) and the superimposed scans of the sensors within the CFRP part as their location changes throughout the different manufacturing steps (the locations of the sensors in the top schematic are mirrored in the bottom plot). c) Quantitative analysis comparing the algebraically calculated and the experimentally measured displacement for each marker.

Having validated the performance of the sensors, they could be used to inform on possible ply defects if the theoretical displacement does not fall within the error of the measured displacement. A digital rendering of the composite and where the sensors are embedded can be seen in Figure S3, Supporting Information. This last figure demonstrates that the proposed sensors can undergo forming and curing of a CFRP piece, while retaining functionality, and yielding valuable information about the relative displacement of plies. These location sensors illustrate the potential for advanced and automated wireless monitoring using seamlessly integrated sensors into composites.

The sensors were covered with 25 µm polyimide tape before embedding to ensure the sensors did not adhere to CFRP and the copper layer and silver trace were not affected by the changes in CFRP. Since the embedded sensors fall below the inclusion size threshold at which structural integrity would be significantly affected by delamination (under 2.5% decrease in compressive strength for delamination smaller than 100 mm^2),[38] the embedded sensors were assumed to have little to no impact on the structural performance of the composite.

Sections of the CFRP containing the embedded sensors were cut in half and imaged using an X-ray and an optical microscope to verify no delamination or defects were present. **Figure 5**a,b shows the cross section of a 7-turn SSNP sensor embedded in CFRP taken with an optical microscope, after cutting the sample in half and polishing it. The embedded sensor can be clearly seen as the dark gray layer in Figure 5a, with the different orientation plies of CFRP showing as lighter layers. The interface between each layer can be seen in Figure 5b; no delamination and minimal defects could be observed between the encapsulating 25 µm polyimide film and the CFRP. The thicker polyimide substrate can be seen at the center of the image, and the coils can be faintly observed in between the thin polyimide wrapping and the thicker substrate. To better observe the coils and any other possible defects, micro-CT X-ray images (Figure 5c,d) were taken. Figure 5c shows the cross section of the cut sensor, the coils can be observed as bright orange lines, the polyimide substrate can be seen in the darker purple areas in between the coils as well as extending slightly past them, since some margin of the substrate was left to avoid damaging the coils. Figure 5d shows the top view of the cut sensor.

Furthermore, it was found that a 9-turn SSNP sensor (the largest manufactured) was 42.5 mg, out of which the polyimide substrate accounted for 42.0 mg. CFRP has a density of 1.6 g cm^{-2};[39] therefore, a 1 m^2 piece of 4 mm thickness would be around 6.4 kg. Assuming a very high sensor load of 34 (1 per ply and 4 references), their total weight would be of 1.4 g, less than 0.02% of the piece weight. This could be reduced by around 99%, or 1.383 g, if the polyimide substrate was removed highlighting the importance of developing directly printable technologies. In any case, as the weight of sensors is below 0.02% their weight penalty on the piece can be assumed negligible.

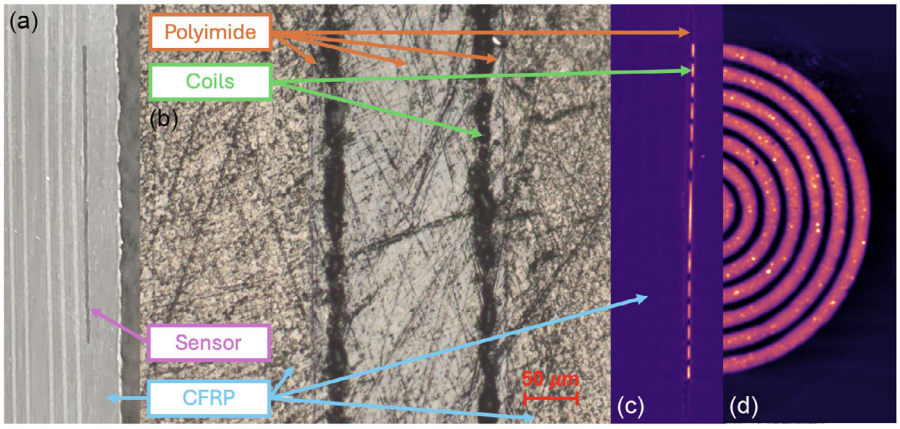

Figure 5. a) Photograph of a cross section of a 7-turn SSNP sensor embedded in composite at; b) cross section of a 7-turn SSNP sensor with 20× optical magnification showing 4 distinct layers (from left to right: CFRP—1 mil polyimide wrapping—polyimide substrate—coils—1 mil polyimide wrapping—CFRP); c) cross section of a micro-CT scan of a 7-turn SSNP sensor, with the coils showing in orange, the polyimide substrate in dark purple and the CFRP in lighter purple; d) top view slice of a micro-CT image of the 7-turn SSNP sensor shown in 5c.

3. Conclusion

A proof of concept for novel passive electromagnetic sensors to be manufactured via the inexpensive and scalable method of screen printing was presented. The printed conductive coils generate a magnetic field when externally excited, allowing for near-field sensing. Various material architectures were evaluated and led to the identification of a sensor platform that has a small footprint, high durability, and performance, as well as good survivability to high temperatures and low pressure used during the curing and forming of CFRP. It was demonstrated that double-sided printing and copper plating increase the signal output, and the combination of both techniques can result in a signal five times larger than that of a control sensor without those enhancements. The manufactured sensors provided valuable insight into ply migration, which was tested by embedding them into primary structural component for aerospace applications. We achieved an accuracy of over 0.6 mm when measuring ply migration, with the ability to read through over 3 mm of CFRP, with sensors varying from 1 to 9 turns, and ranging from 0.5 to 1.5 μm in thickness, depending on the architecture used. Furthermore, accuracy and improvements could be attained with optimized coil shapes and advanced post-processing image analysis. Lastly, the CFRP pieces were cut in half and the cross section of the embedded sensors was scrutinized with optical microscopy and X-ray imaging, revealing no delamination as well as minimal defects.

Future work will involve optimizing sensor accuracy in order to bring it down to 0.15 mm (current testing equipment limit), embedding the sensor directly, without the need for any Kapton tape or polyimide film, and using the sensor for detection of damage in addition to ply migration monitoring.

4. Experimental Section

Screen Printing: Meshtech NBC[40] fabricated the screen with a coil pattern using photoimaged MM1 emulsion (10–14 μm) supported on an SS360 stainless steel mesh. The method to prepare and print silver molecular inks is described elsewhere;[32] the ink is based on silver neodecanoate combined with a polymeric binder, and with a final viscosity of between 5000 and 6000 cP. Polyimide film was chosen as a substrate for its compatibility with the processing conditions used in forming the CFRP, most importantly its chemical and thermal stability. Sensors were prepared by screen printing the molecular ink onto 21.6 cm × 27.9 cm sheets of polyimide film using a flatbed American M&M S-912M[41] small format screen printer.

Postprinting Processing: The silver traces were processed following the methods from Liu et al and Wagner et al.[42,43] which consist of UV curing followed by thermal sintering. To connect both terminals of the sensor, small perforations were made through the polyimide film, and a thin and narrow silver ink trace was deposited with a syringe on the back of the substrate to complete the closed-loop spiral. Then, the curing and sintering process was repeated to make the back-trace conductive. For double-sided sensors, the coils were printed, UV cured, and sintered on both sides of the film, and then, the electrical connections between two coils were made simultaneously through substrate perforations at specific locations.

Copper Plating: For samples that were electrolessly plated with copper, the additional binder was used in the silver ink formulation in comparison to that described in an earlier report.[30,32] The additional binder served to increase the adhesion of the metal trace to polyimide film, but also increased the trace volume resistivity up to 90 μΩ cm from the literature value of 15–45 μΩ cm for pure silver sensors.[32] The silver sensors were submerged in an electroless plating solution for a given amount of time, as per Hibder et al.[44] The solution is based on CuSO4, Rochelle Salts, NaOH, and formaldehyde. Postplating, the sensors were removed from the copper plating solution, rinsed with distilled water, and dried with nitrogen. The copper plating decreased the resistivity of the baseline coils (silver only) by 20–30%. An optimal plating time of 120 min was determined in which sensors could be fabricated uniformly, with high trace thickness and good adhesion. Longer plating times resulted in defects, including flaking, where the trace separates from the substrate; increased surface roughness; copper depositing laterally causing coils to short; and delamination, which occurred when the entire trace separated. Three replicates of each architecture and size of sensor were made to account for manufacturing variances.

Characterization: The sensors were characterized using several techniques. A CT100 Cyber Technologies optical profilometer[45] was used to measure the height, thickness, and surface roughness of the printed sensors. A Bruker 1275 Skyscan X-ray[46] was used to verify any delamination or deformities that could have been caused by the sensor in the CFRP. A saw was used to cut the sample at the location of the sensor, yielding a cross section of the embedded sensor in the composite. Polish was used to ensure the cut surface was clean. Optical microscope images were taken using a ZEISS Stereo Discovery microscope.[47] A Fluke 115

Digital Multimeter with Pomona electronics 6341 tips[48] was used to measure the resistance between the center and the edge of the sensor before bridging both terminals together. The resistance was observed to increase proportionally to the number of turns in a sensor, varying from 4.7 Ω for the 2-turn sensor up to 37.2 Ω for the 9-turn sensor. Lastly, eddy current testing was done to validate performance. This was done using an EC TecView Acquisition and Analysis software and hardware,[49] with a transmit-receive reflection type EC probe consisting of an outer excitation coil and an inner receiver. The frequency tuning of our three-coil (inductor, sensor, and receiver) system was determined experimentally and found to be in the range of 100–250 kHz; subsequently, we used a frequency of 200 kHz to drive the transmitter component of our eddy current probe. The probe was excited with a 200 kHz, 10 V_{pp} sinusoidal waveform, while a 40 dB gain was applied to the receiver signal. The probe was mounted in a robotic arm able to scan a planar (horizontal) test piece at a speed of 12 mm s^{-1}, and a step of 1 mm on both scanning and indexing directions. The measurements were taken at separations (on the vertical axis) varying from 1 up to 4 mm between the sensor's plane and the probe. In addition to the excitation coil, the scanning probe contains an inner, concentric coil, shielded from the excitation one which allows for the reading of the signal from the sensor. The voltage amplitude of the receiving coil is the output used for analysis. This amplitude is expressed as a percentage, based on the recorded orthogonal eddy current signal components, with 100% representing the maximum on a scale of 5 V_{pp}, after application of the gain settings. Since all instrument parameters were kept the same for all scans, the percentage amplitude value allows for quantitative comparison among various experiments.

To measure the effects of composite materials, eddy current scans were performed with sheets of CFRP of varying thicknesses (1, 2, 3, and 4 mm) placed on top of the printed sensors. Measurements were calibrated at a 0 mm separation distance between the probe and sensor followed by measurements taken with 1 mm incremental increases in separation up to 4 mm.

The sensors underwent forming and curing trials. They were embedded during the hand layup deposition of the prepreg plies for the manufacture of a flat preform. Before this, they were wrapped in 1 mil Kapton tape. A standard unidirectional carbon/epoxy composite prepreg (0.135 mm thickness per ply) was used. During the placement of each sensor, the position was marked on a guide sheet to keep a record of its depth of embedment (from 0.135 to 4 mm). The laminates were formed into a desired 3D shape and then cured in an autoclave, at 6 bar, 177 °C for 5 h. Using the eddy current procedure described above, the sensors were interrogated after the preform fabrication, forming and curing steps. The data was then processed with VBA and MATLAB scripts in order to obtain the relative displacement of each sensor.

Supporting Information

Supporting Information is available from the Wiley Online Library or from the author.

Acknowledgements

This research was supported by the Security and Disruptive Technologies division of the National Research Council Canada.

Open Access funding provided by the National Research Council Canada library.

Conflict of Interest

The authors declare no conflict of interest.

Author Contributions

José Barragán: data curation (lead); formal analysis (lead); methodology (lead); writing—original draft (lead); writing—review and editing (lead). **Arnold Kell**: methodology (supporting); supervision (supporting); writing—review and editing (supporting). **Xiangyang Liu**: methodology (supporting). **Seokjee Shin**: investigation (supporting); methodology (supporting). **Catalin Mandache**: data curation (supporting); formal analysis (supporting); investigation (supporting); methodology (supporting); supervision (supporting); validation (supporting); writing—review and editing (supporting). **Drazen Djokic**: conceptualization (equal); data curation (supporting); formal analysis (supporting); investigation (supporting); methodology (equal); visualization (supporting); writing—review and editing (supporting). **Dayna Bennett**: Data curation (supporting); formal analysis (supporting); methodology (supporting); writing—review and editing (lead). **Katherine Houlahan**: data curation (supporting); formal analysis (supporting). **Marc Genest**: conceptualization (equal); project administration (lead); resources (equal); supervision (supporting); writing—review and editing (supporting). **Benoît H. Lessard**: resources (equal); supervision (supporting). **Chantal Paquet**: conceptualization (supporting); supervision (lead); writing—original draft (equal); writing—review and editing (equal).

Data Availability Statement

The data that support the findings of this study are available from the corresponding author upon reasonable request.

Keywords

carbon fiber composites, embedded sensors, near-field sensors, printed electronics

Received: June 5, 2024
Revised: November 25, 2024
Published online: January 10, 2025

[1] B. Ashrafi, M. B. Jakubinek, Y. Martinez-Rubi, M. Rahmat, D. Djokic, K. Laqua, D. Park, K.-S. Kim, B. Simard, A. Yousefpour, *Acta Astronaut.* **2017**, *141*, 57.
[2] S. Erland, T. J. Dodwell, R. Butler, *Composites, Part A* **2015**, *77*, 210.
[3] R. M. A. Khan, I. E. Tabrizi, H. Q. Ali, E. Demir, M. Yildiz, *Polym. Test.* **2020**, *90*, 106653.
[4] G. Mook, J. Pohl, F. Michel, T. Benziger, A. Hilbig, *Materials for Transportation Technology*, Wiley-VCH Verlag GmbH, Weinheim **2000**, p. 198.
[5] R. de Oliveira, C. A. Ramos, A. T. Marques, *Comput. Struct.* **2008**, *86*, 340.
[6] A. Gullapalli, V. Beedasy, J. D. S. Vincent, Z. Leong, P. Smith, N. Morley, *Adv. Eng. Mater.* **2021**, *23*, 2100313.
[7] J. S. Chilles, A. F. Koutsomitopoulou, A. J. Croxford, I. P. Bond, *Compos. Sci. Technol.* **2016**, *134*, 81.
[8] A. Huijer, C. Kassapoglou, L. Pahlavan, *Sensors* **2021**, *21*, 6926.
[9] R. Janeliukstis, D. Mironovs, *Mech. Compos. Mater.* **2021**, *57*, 131.
[10] X. Cheng, X. Cao, Z. Wu, Z. Ying, D. Camilleri, X. Hu, *Adv. Eng. Mater.* **2023**, *25*, 19.
[11] A. Winkler, N. Modler, W.-G. Drossel, T. Mäder, C. Körner, *Adv. Eng. Mater.* **2018**, *20*, 1801001.
[12] Y. Lv, L. Min, F. Niu, Z. Qin, M. Zhang, B. Zhao, Y. Liu, K. Pan, *Adv. Mater. Technol.* **2023**, *8*, 2201886.
[13] A. Winkler, N. Modler, T. Weber, O. Täger, *Adv. Eng. Mater.* **2018**, *20*, 1800588.
[14] T. Karagiannis, E. F. Karachalios, N. D. Alexopoulos, *Mater. Des. Process. Commun.* **2021**, *3*, e191.
[15] Ç. Yılmaz, H. Q. Ali, M. Yıldız, *Polym. Compos.* **2023**, *44*, 2956.

[16] O. Frazão, R. Oliveira, I. Dias, *Microwave Opt. Technol. Lett.* **2009**, *51*, 235.
[17] J. A. Etches, G. F. Fernando, *Polym. Compos.* **2009**, *30*, 1265.
[18] J. A. Etches, G. F. Fernando, *Polym. Compos.* **2010**, *31*, 284.
[19] J. Missinne, N. Teigell Benéitez, A. Lamberti, G. Chiesura, G. Luyckx, M.-A. Mattelin, W. Van Paepegem, G. Van Steenberge, *Adv. Eng. Mater.* **2018**, *20*, 1701127.
[20] M. Majumder, T. K. Gangopadhyay, A. K. Chakraborty, K. Dasgupta, D. K. Bhattacharya, *Sens. Actuators, A* **2008**, *147*, 150.
[21] S. Geller, T. Tyczynski, M. Gude, S. Sauer, W.-J. Fischer, *Adv. Eng. Mater.* **2018**, *20*, 1800447.
[22] D. Barazanchy, M. Martinez, B. Rocha, M. Yanishevsky, *J. Sens.* **2014**, *2014*, 1.
[23] M. K. Idris, J. Qiu, G. W. Melenka, G. Grau, *Eng. Res. Express* **2020**, *2*, 025022.
[24] S.-J. Joo, M.-H. Yu, E.-B. Jeon, H.-S. Kim, *Compos. Sci. Technol.* **2017**, *142*, 189.
[25] E.-B. Jeon, T. Fujimura, K. Takahashi, H.-S. Kim, *Composites, Part A* **2014**, *66*, 193.
[26] C. Mandache, R. Desnoyers, Y. Bombardier, *Sensors* **2022**, *22*, 9958.
[27] R. J. Ditchburn, S. K. Burke, *NDT&E Int.* **2005**, *38*, 690.
[28] K. Koyama, H. Hoshikawa, G. Kojima, *J. Pressure Vessel Technol.* **2013**, *135*, 041501.
[29] T. Wang, D. Wu, W. Chen, J. Yang, *Compos. Struct.* **2021**, *268*, 114012.
[30] A. J. Kell, K. Wagner, X. Liu, B. H. Lessard, C. Paquet, *ACS Appl. Electron. Mater.* **2024**, *6*, 1.
[31] J. H. Huang, P. S. Shih, V. Renganathan, S. J. Gräfner, Y. A. Chen, C. H. Huang, C. L. Kao, Y. S. Lin, Y. C. Hung, C. R. Kao, *Electrochim. Acta* **2022**, *425*, 140710.
[32] A. J. Kell, C. Paquet, O. Mozenson, I. Djavani-Tabrizi, B. Deore, X. Liu, G. P. Lopinski, R. James, K. Hettak, J. Shaker, A. Momciu, J. Ferrigno, O. Ferrand, J. X. Hu, S. Lafrenière, P. R. L. Malenfant, *ACS Appl. Mater. Interfaces* **2017**, *9*, 17226.
[33] D. C. Giancoli, *Phys. Educ.* **2000**, *35*, 370.
[34] S. Tumanski, *Meas. Sci. Technol.* **2007**, *18*, R31.
[35] N. Angelidis, C. Y. Wei, P. E. Irving, *Composites, Part A* **2004**, *35*, 1135.
[36] E. Dilonardo, M. Nacucchi, F. De Pascalis, M. Zarrelli, C. Giannini, *Compos. Sci. Technol.* **2020**, *192*, 108093.
[37] T. Liang, W. Ren, G. Y. Tian, M. Elradi, Y. Gao, *Compos. Struct.* **2016**, *143*, 352.
[38] Y. Zhang, K. Huang, R. Sun, F. Liao, L. Guo, L. Zhang, *Compos. Struct.* **2022**, *281*, 115063.
[39] M. A. El-Reedy, *Asset Integrity Management for Offshore and Onshore Structures*, Gulf Professional Publishing is an imprint of Elsevier, Cambridge, MA **2022**, p. 199.
[40] NBC Meshtech Americas **2023**.
[41] ATW **2022**.
[42] K. Wagner, S. Zou, Y. Martinez-Rubi, A. J. Kell, C. Paquet, B. H. Lessard, *FPE* **2023**, *8*, 25005.
[43] X. Liu, D. Li, H. Fukutani, P. Trudeau, L. Khoun, O. Mozenson, K. L. Sampson, M. Gallerneault, C. Paquet, T. Lacelle, B. Deore, O. Ferrand, J. Ferrigno, P. R. L. Malenfant, A. J. Kell, *Adv. Electron. Mater.* **2021**, *7*, 2100194.
[44] P. C. Hidber, P. F. Nealey, W. Helbig, G. M. Whitesides, *Langmuir* **1996**, *12*, 5209.
[45] Snowhouse **2024**.
[46] Bruker **2024**.
[47] ZEISS **2024**.
[48] Fluke, *Fluke* **2020**
[49] TecScan **2023**.

